Investigation of Velocity Boundary Conditions in Counterflow Flames

Woe-Chul Park*
Department of Safety Engineering, Pukyong National University, Pusan 608-739, Korea
Anthony Hamins
Building and Fire Research Laboratory, National Institute of Standards and Technology, Gaithersburg, MD 20899-8663, U. S. A.

The effects of velocity boundary conditions on the structure of methane-air nonpremixed counterflow flames were investigated by two-dimensional numerical simulation. Two low global strain rates, 12 s^{-1} and 20 s^{-1}, were considered for comparison with measurements. Buoyancy was confirmed to have strong effects on the flame structure at a low global strain rate. It was shown that the location where a top hat velocity profile was imposed is sensitive to the flame structure, and that the computed temperature along the centerline agrees well with the measurements when plug flow was imposed at the inner surface of the screen nearest the duct exit.

Key Words: Velocity Boundary Conditions, Plug-Flow, Screens, Two Dimensional Simulation, Mixture Fraction Combustion Model, Air-Methane Counterflow Flame

Nomenclature

a_g : Global strain rate
D : Duct diameter
L : Duct separation
r_v : Velocity ratio, V_O/V_F
s : Distance between duct exit and location where top hat velocity profile is imposed
T : Temperature
V : Mean velocity in duct
subscripts
O : Oxidizer
F : Fuel

1. Introduction

A counterflow diffusion flame is formed between two opposed ducts, the oxidizer duct and the fuel duct. To remove a large scale structure and to achieve a uniform velocity distribution over the cross-sectional area, a set of screens, sintered metals or flow straighteners is inserted in the ducts. In most experimental studies, these screens are located not at the duct exits but at a distance from the exit, to retain the screens, or to get a stable flame (Maruta et al., 1998 and Lee et al., 1996). Chelliah et al. (1990) investigated the velocity boundary conditions at the duct exit by assuming either potential flow or plug flow. They showed that the plug flow boundary condition agrees well with measurements.

A top hat velocity profile based on the plug flow assumption has been widely used as a boundary condition in one-dimensional flame codes like OPPDIF (Luts et al., 1997). Park (2001) and Park et al. (2001) showed that the results of two-dimensional simulation of axisymmetric counterflow flames, with the plug flow boundary condition at the duct exit, agreed very well with those of OPPDIF. The velocity boundary conditions at the duct exit in both the

* Corresponding Author,
E-mail : wcpark@pknu.ac.kr
TEL : +82-51-620-1520; **FAX** : +82-51-620-1516
Department of Safety Engineering, Pukyong National University, Pusan 608-739, Korea. (Manuscript **Received** August 3, 2001; **Revised** December 3, 2001)

one- and two-dimensional simulations were the plug flow. However, when the screens are located at a distance from the exit, the velocity profile at the duct exits will not be uniform, and a special care shald be takan for the velocity boundary condition. Motivation of the present study is that it is necessary to find how much the location of the screens in the duct impacts the flame structure, and to find where the plug flow boundary condition should be imposed in numerical simulation. The hypothesis is that imposing the top hat velocity profile at the location of the inner surface of the screen nearest the duct exit is valid since the velocity at the screen surface is expected to be uniform. The first objective of this numerical study is to investigate sensitivity of the location where the top hat velocity profile is imposed on the flame structure. The second is to suggest an appropriate location of the plug flow boundary condition for the screens.

The NIST Fire Dynamics Simulator (FDS) (McGrattan et al., 2001), applicable to unsteady three-dimensional fire problems, is used in the present study, on the basis of previous validation investigations (Park, 2001 and Park et al., 2001). Results of the temperature profile along the centerline were compared with measurements.

2. Methodology

The experimental apparatus is shown in Fig. 1. Methane diluted by nitrogen flows in the fuel duct, and undiluted air in the oxidizer duct. The flame, formed between the two ducts separated by 25 mm, is shielded from ambient air by nitrogen gas.

Figure 2 represen the dimensions of the duct and screens. The inside diameter at the duct exit and the outside diameter of two ducts are 23 mm and 28 mm, respectively. There is a set of three screens inside each duct. The distance between the duct exit and the face of the first screen is 1.6 mm, and the total height of the screen set is 4 mm. Three 1.6 mm thick rings retain the screens. The open porosity of each screen is 35%.

Temperature along the centerline (y-axis) was measured using a thermocouple for two low

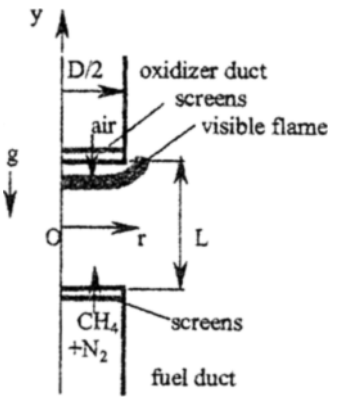

Fig. 1 A schematic diagram of the counterflow ducts and notations

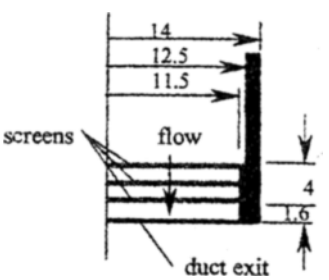

Fig. 2 Dimensions of the screens and the duct near the exit in mm, nonscale

global strain rates, 12 s^{-1} and 20 s^{-1}. The global strain rate, a_g, is defined as (Seshadri and Williams, 1978)

$$a_g=\frac{2V_O}{L}\left[1+\frac{V_F}{V_O}\left(\frac{\rho_F}{\rho_O}\right)^{0.5}\right] \tag{1}$$

where V_O is the mean velocity in the oxidizer duct, V_F is the mean velocity in fuel duct, ρ_A is the density of air and ρ_F is the density of fuel (mixture of methane and nitrogen).

The fuel composition and velocity for each global strain rate are listed in Table 1. When $a_g=$ 12 s^{-1} and the velocity ratio, $r_v=1$, the flame is located close to the top oxidizer duct. To avoid problems associated with heat conduction from the flame to the duct, $r_v=4$ was chosen.

The governing equations for a laminar diffusion flame are as follows:

$$\frac{\partial\rho}{\partial t}+\frac{\partial\rho u_i}{\partial x_i}=0 \tag{2}$$

Table 1 Composition of fuel and mean velocity in the ducts to be investigated

a_g (s^{-1})		12	20
Fuel (%)	CH_4	17.8	20
	N_2	82.2	80
V_O (m/s)		0.121	0.129
V_F (m/s)		0.030	0.129
r_v		4	1

$$\frac{\partial \rho u_i}{\partial t}+\frac{\partial \rho u_i u_j}{\partial x_j}=-\frac{\partial p}{\partial x_i}+\rho g_i+\frac{\partial \tau_{ij}}{\partial x_j} \quad (3)$$

$$\frac{\partial \rho h}{\partial t}+\frac{\partial \rho h u_i}{\partial x_i}-\frac{Dp}{Dt}=Q+\frac{\partial}{\partial x_i}\left(\lambda \frac{\partial T}{\partial x_i}\right)+\frac{\partial (u_i \tau_{ij})}{\partial x_i} \quad (4)$$

$$\frac{\partial \rho Y_i}{\partial t}+\frac{\partial \rho Y_i u_j}{\partial x_j}=\frac{\partial}{\partial x_j}\left(\rho D_i \frac{\partial Y_i}{\partial x_j}\right)+w_i \quad (5)$$

where, u is the velocity, τ is the shear stress, and p is the pressure. h represents the enthalpy, Q the heat release rate per unit volume, λ the thermal conductivity, T the temperature, Y the species mass fraction, D the diffusion coefficient, and w the chemical production rate per unit volume. The thermal radiation is not included in the present study.

In the NIST Fire Dynamics Simulator (FDS) (McGrattan et al., 2001), both the direct numerical simulation (DNS) and large eddy simulation (LES) have been employed. In this study, DNS was chosen since it is more appropriate than LES for small laboratory scale experiments. Park (2001) showed that the mixture fraction combustion model (Floyd et al., 2001) employed in FDS was in good agreement with the one-dimensional counterflow flame code OPPDIF (Luts et al., 1997). The mixture fraction combustion model provides the local heat release rate, temperature and flame shape without detailed chemical kinetics. For mixture fraction combustion model was used. The numerical method and solution procedures including the mixture combustion model are described in detail in McGrattan et al. (2001).

The top hat velocity profile was imposed at 0 mm (the duct exits), 5 mm and 10 mm, respectively, from the duct exit for each global strain rate, to see the sensitivity of the location of the top hat velocity on the flame structure. The magnitude of the top hat velocity profile is the mean velocity, that is, the volume flowrate divided by the cross-sectional area of the duct. The computational domain was taken to be 40 mm x 70 mm, and 80x140 grids (a uniform grid size, 0.5 mm in the both r- and y-directions) were used on the basis of the validation tests (Park, 2001 and Park et al., 2001). The computed flames reached a steady state after 0.7 s from start of computation. Computation up to 1.0 s required about 100 min on a PC with PIII-650Mhz CPU and 258 MB RAM.

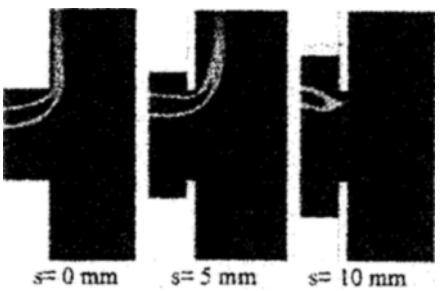

Fig. 3 High temperature reaction zone for steady flames of a_g=12 s^{-1} for different values of s

3. Results and Discussion

When the top hat velocity profile is imposed at a distance (s) inside the duct from its exit, the no-slip boundary conditions on the duct wall increases velocity in the y-direction although it is negligible for a short distance. On the other hand, buoyancy due to a high temperature flame increases velocity in the r-direction near the duct exit. The top hat velocity profile has no radial component, but at the duct exit the velocity profile has both the axial and radial components due to the momentum deficit near the duct wall and the buoyancy force. To confirm this, flames of three different values of s at a_g=12 s^{-1} and r_v=4 were compared in Fig. 3. The flame rises around the duct by the buoyancy, and its shape varies with s. The flame also shows that velocity in the r-direction is not zero when s=5 mm and 10 mm. The velocity components at the duct exit can be investigated from plotted velocity vectors.

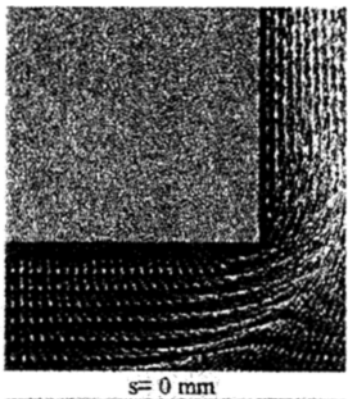

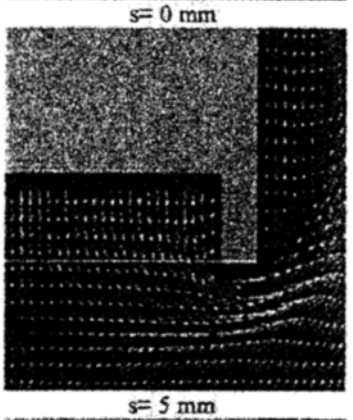

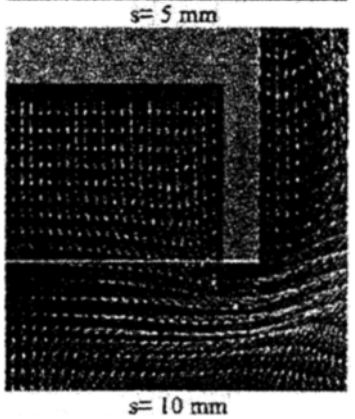

Fig. 4 Velocity vectors around the oxidizer duct exit at ag=12 s^{-1} for different values of s

Figure 4 depicts velocity vectors around the oxidizer duct exit. Velocity at 0 mm (duct exit), 5 mm, and 10 mm from the exit is uniform where the top hat velocity profile was given, but varies as air flows towards the duct exit. The axial velocity at the center of the duct decreases with increasing s, and is nearly zero when s=10 mm. The decreasing axial velocity increases the radial

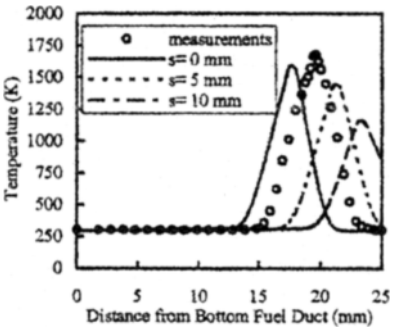

Fig. 5 Comparison of temperature profile along the y-axis at a_g=12 s^{-1}

velocity at the duct exit, and that a recirculation region is formed outside the duct when s=5 mm and 10 mm. This clearly shows that, when the screens locate in the duct at 5 mm or 10 mm from the exit, the velocity profile at the exit is not uniform, and therefore assuming it a top hat velocity profile may cause a severe error as can be confirmed by the following comparison of temperature distribution with measurements.

The corresponding temperature profiles along the y-axis were compared in Fig. 5. When s=0, that is, the velocity profile at the duct exit is of top hat, the simulated flame position is lower than the measurements where the nearest screen is at 1.6 mm from the exit as seen in Fig. 2: the peak temperature at 17.5 mm in simulation, and 19.6 mm in the measurements from the fuel duct. This implies that the top hat velocity at the duct exit gives a large error. The flame position moves towards the upper oxidizer duct and the peak temperature decreases with increasing s as compared in Table 2. As expected from Fig. 3, the peak temperature at s=10 mm is much lower than that of s=0, and a part of the flame is inside the duct when s=10 mm. The decrease in the axial velocity with increasing s shown by the velocity vectors in Fig. 4 shifted the flame position. The measured temperature profile exists between the two simulated temperature profiles at s=0 and s=5 mm. This indicates that the top hat velocity profile must be given at $0<s<5$ mm, and that the flame structure is highly sensitive to the location of the screens.

Table 2 Comparison of computed T_{max} and its location for $a_g=12\ s^{-1}$

s (mm)	T_{max} (K)	location of T_{max} (mm) *
0	1587	17.5
5	1431	21.5
10	1060	24.0

* distance from fuel duct

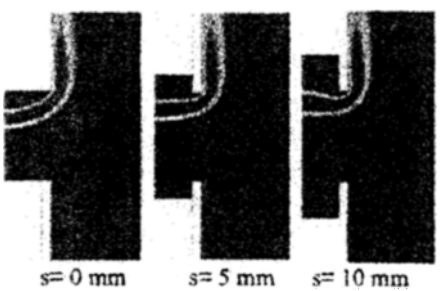

Fig. 6 High temperature reaction zone for steady flames of $a_g=20\ s^{-1}$ for different values of s

The effects of the velocity boundary conditions on the flame structure were further investigated for the case of a higher global strain rate ($a_g=20\ s^{-1}$, $r_v=1$). The magnitude of the top hat velocity at both ducts is 0.129 m/s, which is a small increase in the air flow, but a large increase in the fuel stream compared to the $a_g=12\ s^{-1}$ case (see V_O and V_F in Table 1).

Figure 6 compares the flames at $a_g=20\ s^{-1}$. The increase of fuel stream yields flames large than the $a_g=12\ s^{-1}$ case in Fig. 3. Changes in the location where the top hat velocity profile is imposed also yield different flame shapes. As seen in the previous case, an increase in the radial velocity and decrease in the axial velocity at the duct exit are clearly observed near the duct exit.

Figure 7 depicts velocity vectors around the exit of the oxidizer duct at $a_g=20\ s^{-1}$. Although the velocity components in the r- and y-directions do not vary with s as much as in the case of $a_g=12\ s^{-1}$ where flame is more sensitive to the buoyancy force, it shows that the y-direction velocity at the center of duct exit becomes weaker with increasing s, the distance from the duct exit to the location where the top hat velocity profile

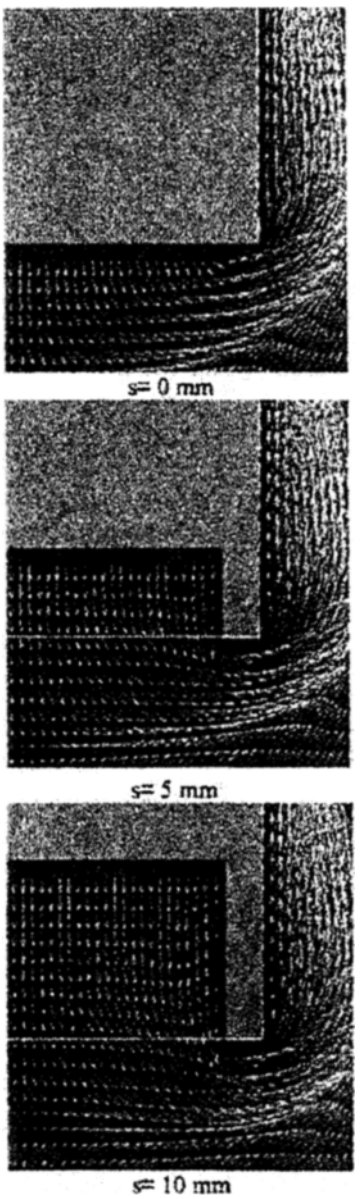

Fig. 7 Velocity vectors around the oxidizer duct exit at $a_g=20\ s^{-1}$ for different values of s

is imposed. This results in shift of the flame position towards the top oxidizer duct as s increases.

The shift of the flame position with s is compared in Fig. 8. The flame position switches with the location of the top hat velocity similarly to the previous case (Fig. 4). Quantitatively, in Table 3, it can be seen that the flame position

Table 3 Comparison of computed T_{max} and its location for $a_g=20\ s^{-1}$

s (mm)	T_{max} (K)	location of T_{max} (mm) *
0	1692	17.5
5	1698	20.5
10	1725	22.0

* distance from fuel duct

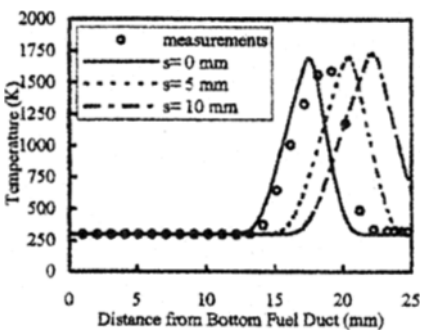

Fig. 8 Comparison of temperature profile along the y-axis at $a_g=20\ s^{-1}$

moves towards the oxidizer duct and the maximum temperature increases as s increases. As seen in the case of $a_g=12\ s^{-1}$, the measured temperature profile locates between the computed profiles of s=0 and s=5 mm. It is confirmed again that the velocity profile at the duct exits is not uniform when the set of screens locates at a distance from the duct exit.

Comparisons of flames (Figs. 3 & 6), velocity vectors abound the oxidizer duct exit (Fig. 4 & 7), temperature profiles (Figs. 5 & 8) and flame temperature and locations (Tables 2 & 3) clearly show that the flame structure at the higher global strain rate is less sensitive to the location where the top hat velocity profile is imposed. From these comparisons it is also confirmed that the buoyancy force has stronger effects on flame at a low global strain rate than flame at a higher global strain rate, since velocity in the ducts increases with the global strain rate.

In both cases a significant impact of the location of the screens on the flame structure was confirmed. When the top hat velocity profile was imposed inside the duct (s>0), the velocity profile at the duct exit was no longer uniform due to the effects of the fluid viscosity and buoyancy. When the top hat velocity profile is given at s>0, the flow develops towards the duct exit by the presence of viscosity, and the buoyancy force strongly affects the flame structure at the low strain rates. The flow development in the duct and buoyancy have contradicting effects in varying the velocity profile: the momentum deficit due to the fluid viscosity increases the axial velocity near the center of the duct, while the buoyancy force increases the radial velocity at the duct exits. The increasing r-direction velocity component at the duct exit implies that buoyancy has strong effects on the flame structure at low global strain rates.

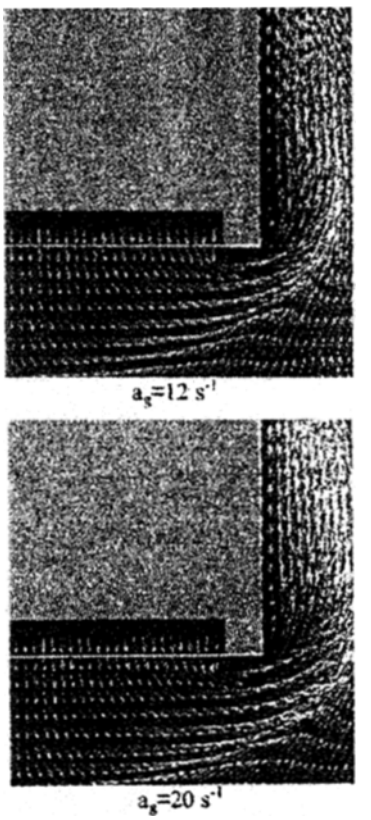

Fig. 9 Velocity vectors around the oxidizer duct exit (s=2 mm)

Assuming the velocity at 2 mm inside the ducts is uniform, where the inner surface of the nearest screen from the duct exit is located (see Fig. 2), the top hat velocity profile was imposed at 2 mm

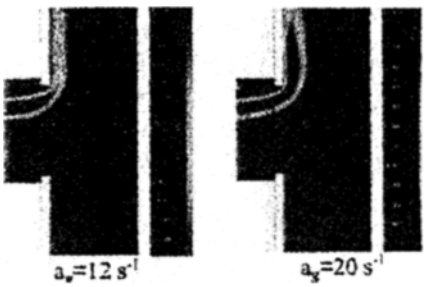

Fig. 10 High temperature reaction zone for steady flames (s=2 mm)

from the exit (s=2 mm). Figure 9 shows velocity vectors around the oxidizer duct exit when s=2 mm. The velocity vectors of the two global strain rates are similar each other because there is a small difference in the velocity of air and s is not large.

Figure 10 is the computed flames for the two global strain rates when the top hat velocity profile is given at 2 mm from the duct exits (s= 2 mm). Flames rise upwards, and are located not at the midplane between the oxidizer and fuel ducts but near the oxidizer duct due to the presence of buoyancy. The buoyancy force affects strongly the flames at the lower strain rates, and this is confirmed by flame at a_g=12 s^{-1} which is positioned close to the oxidizer duct even the velocity ratio V_O/V_F is 4. At moderate and high strain rates, a higher velocity ratio at a given global strain rate increases the velocity in the oxidizer duct and shifts flame towards the fuel duct.

Figure 11 compares the flame obtained by computation with the experimental image taken by a digital camera. Both curvatures of the flames agree well. Unfortunately, the digital image at a_g=12 s^{-1} was not taken.

In Fig. 12, the temperature distribution along the centerline (y-axis) was compared. The computed temperature profiles with the plug flow assumption at s=2 mm are in good agreement with measurements in the both cases. In addition to the agreement in flame shape in Fig. 11, this confirms quantitatively that imposing the top hat velocity profile at the inner surface of the screen nearest the duct exit yields good results.

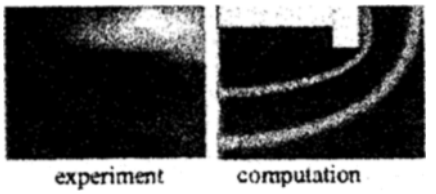

Fig. 11 Comparison of flames at a_g=20 s^{-1} (s=2 mm)

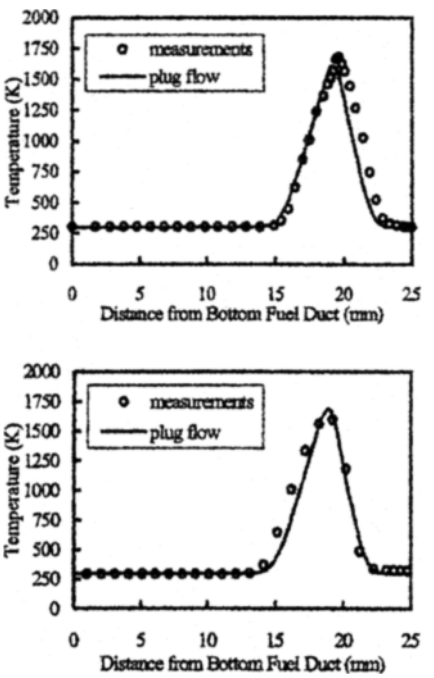

Fig. 12 Temperature profile along the y-axis for a_g=12 s^{-1} (top) and 20 s^{-1} (bottom), s=2 mm

Conclusions

The velocity boundary conditions for methane-air counterflow diffusion flames were investigated numerically at two low global strain rates, a_g=12 s^{-1} and 20 s^{-1}. Flames, velocity vectors and temperature distribution along the centerline with the plug flow assumption were compared. From the results the following conclusions may be drawn:

(1) The location where the top hat velocity profile is imposed has strong influence on the flame structure.

(2) When the screen is not located at the duct exit, the velocity profile at the exit is not uniform

and hence the plug flow assumption at the exit yields incorrect results at a low global strain rate.

(3) Due to the presence of buoyancy the radial velocity increases and the axial velocity decreases at the duct exit with increasing distance from the duct exit to the screen.

(4) It was confirmed that the buoyancy force affects the flame structure more significantly at a lower global strain rate.

(5) The top hat velocity profile imposed at the location of the inner surface of the screen nearest the duct exit agreed well with measurements.

Acknowledgement

The authors are grateful to Dr. Kevin McGrattan and Dr. Mattew Bundy for helpful discussions.

References

Chelliah, H. K., Law, C. K., Ueda, T., Smoke, M. D. and Williams, F. A., 1990, "An Experimental and Theoretical Investigation of the Dilution, Pressure and Flow-Field Effects on the Extinction Condition of Methane-Air-Nitrogen Diffusion Flames," *Proc. 23rd Symposium on Combustion*, pp. 503~511.

Floyd, J. E., McGrattan, K. B. and Baum, H. R., 2001, "A Mixture Fraction Combustion Model for Fire Simulation Using CFD," *Proc. Int'l Conf. on Engineered Fire Protection Design*, pp. 279~290.

Lee, K. Y., Cha, D. J., Hamins, A. and Puri, I. K., 1996, "Heat Relaease Mechanisms in Inhibited Laminar Counterflow flames," *Combustion and Flames*, Vol. 105, pp. 27~40.

Maruta, K., Yoshida, M., Guo, H., Ju, Y. and Niioka, T., 1998, "Extinction of Low-Stretched Diffusion Flame in Microgravity," *Combustion and Flames*, Vol. 112, pp. 181~187.

McGrattan, K. B., Baum, H. R., Rehm, R. G., Hamins, A., Forney, G. P., Floyd, J. E., Hostikka, S., 2001, Fire Dynamics Simulator Technical Reference Guide V. 2, National Institute of Standards and Technology, Gaithersburg, MD (also http://fire.nist.gov/fds/).

Park, W. C., 2001a, "An Evaluation of a Direct Numerical Simulation for Counterflow Diffusion Flames," Submitted to Korea Institute for Industrial Safety Journal (in Korean).

Park, W. C., Hamins, A. and McGrattan, 2001, "Two-Dimensional Simulation of Diluted Nonpremixed Counterflow Flames," Submitted to 29th Int'l Symposium on Combustion.

Puri, I. K. and Hamins, A., 2001, "A Numerical Investigation of Radiative Effects in Near-Extinction Methane-Air Nonpremixed Flames," Submitted to Combustion and Flame.

Seshadri, K. and Williams, F. A., 1978, "Laminar Flow Between Parallel Plates with Injection of a Reactant at High Reynolds Number," *Int'l J. Heat Mass Transfer*, Vol. 21, pp. 251~253.